Macromolecules

ARTICLE

pubs.acs.org/Macromolecules

Composition Effect on Interplay between Phase Separation and Dewetting in PMMA/SAN Blend Ultrathin Films

Jichun You,[†,‡] Yonggui Liao,[§] Yongfeng Men,[‡] Tongfei Shi,[*,‡] Lijia An,[*,‡] and Xiuhong Li[⊥]

[†]College of Material Chemistry and Chemical Engineering, Hangzhou Normal University, Hangzhou 310036, China

[‡]State Key Laboratory of Polymer Physics and Chemistry, Changchun Institute of Applied Chemistry, Chinese Academy of Sciences, Changchun 130022, China

[§]School of Chemistry and Chemical Engineering, Huazhong University of Science and Technology, Wuhan 430074, China

[⊥]SSRF, Shanghai Institute of Applied Physics, Chinese Academy of Sciences, Shanghai 201800, China

ABSTRACT: Using *in situ* atomic force microscopy (AFM) and grazing incidence ultrasmall-angle X-ray scattering (GIUSAX), the composition dependence of phase separation, dewetting, and interplay between them in blend [poly(methyl methacrylate) (PMMA) and poly(styrene-*ran*-acrylonitrile) (SAN)] ultrathin films ($\sim 1R_g$, radius of gyration) on silicon oxide substrate was investigated. It was found that phase behaviors depended crucially on the composition in blend. First, dewetting morphologies in SAN50 and SAN70 were still under the control of U_{q0}/E, which was introduced in our previous work [Polymer 2009, 50, 4456] to distinguish different dewetting pathways. Here, U_{q0} and E described the initial amplitude of the surface undulation and original thickness of film, respectively; second, composition produced significant influences on its gradient in composition fluctuation, resulting in the accelerated (or suppressed) dewetting; last, this kind of acceleration or suppression affected the following interplay between phase separation and dewetting so much. Using two samples of "dewetting/wetting−phase separation" and "wetting−dewetting/phase separation" with different components, we discussed the interplay mechanism of them in detail. In conclusion, our results indicate that dewetting, phase separation, and the following interplay between them are sensitive to composition in blend. Furthermore, composition gradient plays an important role in them.

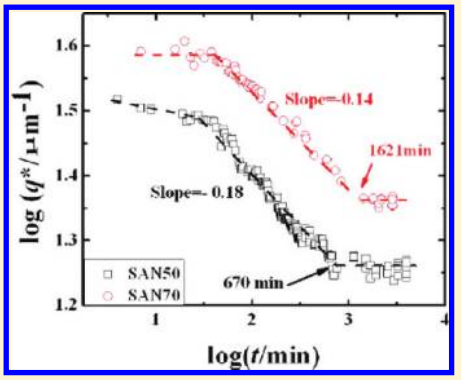

INTRODUCTION

Phase behaviors in polymer blend (ultra)thin films have been a focus of scientific interest over recent years since these films play an important role in many applications.[1−4] On one hand, much attention has been paid to phase separation since they are blends. These results indicated that the composition of the blend affected both mechanism and kinetics of phase separation.[5−9] In thermodynamics, it is well-known that we can get bicontinuous structures and island of one polymer in the continuous phase of the other by varying the component from critical to off-critical.[10] In kinetics, several exponents (e.g., 0, 1/3, and 2/3) which were introduced to describe growth of phase-separated rich domain were predicted and validated by theory and experiment, respectively, with different component.[11−13] There have been some reports on phase separation in the case of confinement also, which is significant to control phase-separated structures in dewetted droplets when dewetting takes place first.[14,15] However, it was a big challenge to detect these structures by general methods because they were buried in some separated droplets until grazing incidence small-angle X-ray scattering (GISAXS) was employed.[16]

On the other hand, much effort has been made on dewetting of them since they are films. For instance, Wensink et al.[17] predicted a new dewetting mechanism named composition fluctuation which has been validated by experiment.[18] Furthermore, composition dependence of dewetting pathway was investigated in miscible PMMA/SAN blend films at 145 °C. Results of that work indicated that the dewetting pathway depended crucially on composition in the blend.[19] Two kinds of dewetting pathways including "fragment of bicontinuous structures", "expansion of holes", and transitional pathway between them were obtained in PMMA/SAN films with different components. Furthermore, a new parameter U_{q0}/E, which described initial amplitude of the surface undulation and original thickness of film, respectively, was employed to distinguish different dewetting pathways. This parameter has been validated by single-component polystyrene (PS)[20,21] as well as miscible and immiscible blend films.[19,22] It indicates that there are two methods to control dewetting pathway: varying amplitude of the surface undulation and initial films thickness. Obviously, the former is under the control of composition in blend, which is the embodiment of composition influence on dewetting.

Received: January 17, 2011
Revised: April 8, 2011
Published: June 10, 2011

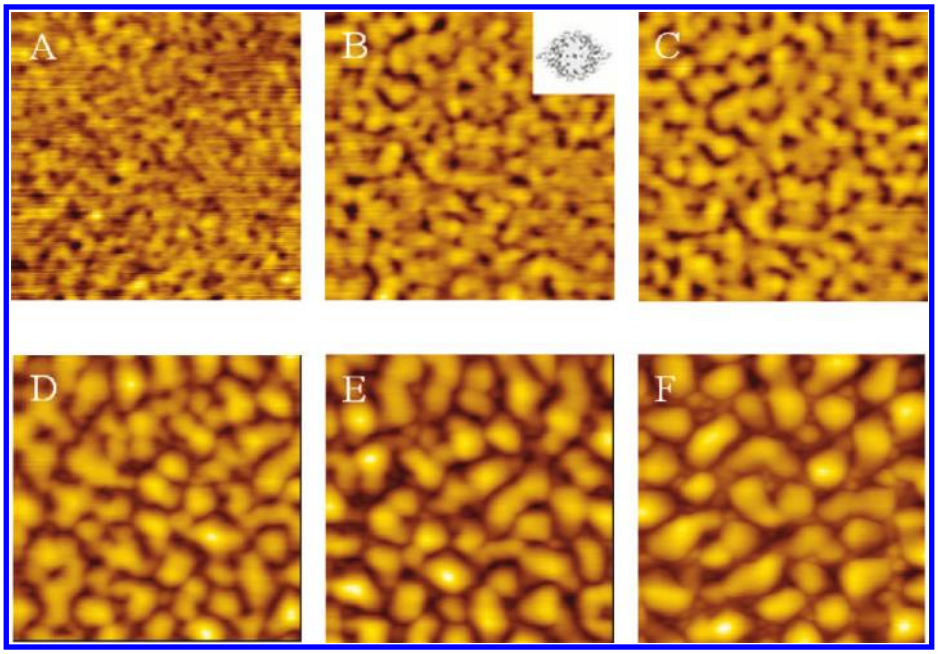

Figure 1. Snapshots of topography images for sample of SAN50 annealed at 155 °C for (A) 6, (B) 35, (C) 55, (D) 209, (E) 556, and (F) 4017 min. The dimensions and the *z*-axes values for topography images are 2 × 2 μm^2 and 25.7 nm, respectively. Inset in image B is the fast Fourier transition (FFT) from corresponding image.

In immiscible polymer blend ultrathin films, there have been some reports on phase separation of blend and dewetting of film. However, most of them focused on the system in which phase separation took place much earlier than dewetting. This results in the absence of investigation of interplay between them.[23] In the PMMA/SAN blend system,[18] however, it was found that dewetting of the whole film (PMMA/SAN) occurred before phase separation in the dewetted droplets for the first time (SAN50 at 175 °C). Therefore, it is so necessary to investigate the interplay between them due to the comparable relative rates.[22] To our knowledge, however, only a few reports focus on this. Results of Ogawa and our previous work indicated that transition from one interplay mechanisum to the other can be carried out by varying film thickness.[22,24] It is worth to notice that composition of blend produces great effect on both phase separation and dewetting in polymer blend films. Relative to miscible blend, occurrence of phase separation makes the movement of polymer chains easier, leading to higher sensitivity of phase behaviors to composition. Therefore, it is reasonable to expect that interplay between them is also sensitive to composition. However, there is no report on this so far. In this work, phase behaviors in PMMA/SAN blend ultrathin films with different components were investigated by *in situ* AFM and GIUSAX. We try to clarify how composition affects phase separation, dewetting, and the following interplay between them.

EXPERIMENT

Materials. The polymer system is a blend of poly(methyl methacrylate) (PMMA) (M_w = 387 kg/mol, PD = 3.72) and ploy(styrene-*ran*-acrylonitrile) (SAN) (M_w = 149 kg/mol, PD = 2.66, 30 wt % of AN) purchased from Acros and Aldrich, respectively. There must be some influence on dewetting and phase separation since both of them are broadly distributed.[25,26] Therefore, we used the same polymers with our previous work.[19,22] SAN was purified by method discussed elsewhere.[27] The radii of gyration (R_g) of an unperturbed chain of PMMA and SAN used in this work are 9.2 and 7.5 nm, respectively.

Sample Preparation. Ultrathin blend films were prepared by spin-coating 1,2-dichloroethane solution of PMMA/SAN (70:30, 50:50, and 30:70 wt %) onto the silicon wafer. Three samples labeled as SAN30, SAN50, and SAN70 were obtained, respectively. Prior to spin-coating, the silicon wafers were cleaned in a bath of 100 mL of 80% H_2SO_4, 35 mL of 30% H_2O_2, and 15 mL of deionized water at 80 °C for 60 min and rinsed in deionized water and then blown-dried with compressed nitrogen. Thicknesses of polymer film and silicon oxide layer measured by D8 Discover X-ray reflectometer (Bruker, Germany) were 9.7 ± 0.2 and 2.0 ± 0.3 nm, respectively.

AFM and GIUSAX Measurements. The *in situ* topography and phase images were obtained simultaneously using an SPA-300 HVA (Seiko Instruments Inc., Japan) at 145 and 155 °C with a temperature-control stage driven in tapping mode.[18] A silicon tip purchased from Olympus was used. Its spring constant, resonance frequency, and radius of curvature are 42 N/m, 340 kHz, and 10 nm, respectively. Synchrotron GIUSAX measurements were performed at BW4 beamline at HASYLAB (DESY, Hamburg, Germany). The energy of the X-ray radiation was 8.979 keV, resulting in a wavelength of 0.138 08 nm. The size of the primary X-ray beam at the sample position was 0.4 × 0.4 mm^2. The sample−detector distance was 13037 mm, resulting in GIUSAXS geometry. In this geometry, at a very large sample−detector distance a high resolution of 2.75 × 10^{-4} nm^{-1} was achieved. X-ray scattering intensity patterns were acquired for 900 s by a two-dimensional detector array (2048 × 2048 pixels). Prior to measurement of GIUSAX, all samples were annealed at 145 and 155 °C for different times in the oven, respectively.

RESULTS AND DISCUSSION

Phase Behaviors in SAN50 and SAN70. First of all, it is necessary to assess the miscibility of PMMA and SAN in the sample of SAN50 and SAN70 at 155 °C. Phase-separated structures in dewetted droplets detected by GIUSAX in SAN50 have

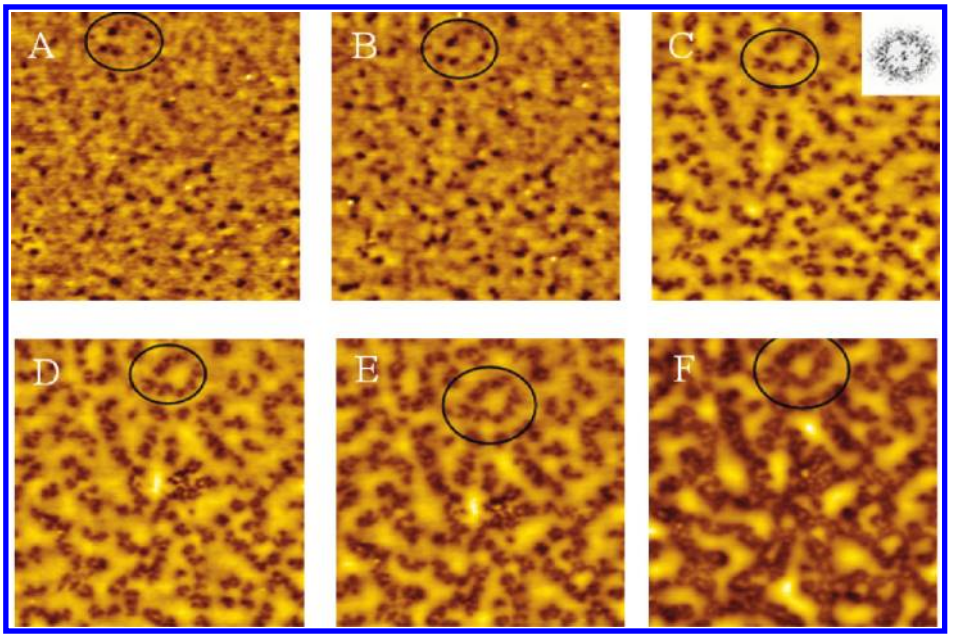

Figure 2. Snapshots of topography images for sample of SAN70 annealed at 155 °C for (A) 23, (B) 78, (C) 291, (D) 443, (E) 725, and (F) 2874 min. The dimensions and the *z*-axes values for topography images are 2 × 2 μm^2 and 28.3 nm, respectively. Inset in image C is the fast Fourier transition (FFT) from corresponding image.

been reported.[19] In SAN70, phase separation of PMMA/SAN takes place also, which is confirmed by GIUSAS in the same way. This is the functional stone of our discussion on interplay between phase separation and dewetting. GIUSAX data will be shown in the following part since we will discuss phase separation in detail.

Figure 1 shows topography images of SAN50 annealed at 155 °C for different times. There are some bicontinuous structures including long hills and gullies when our sample is annealed for 6 min (Figure 1A). These hills and gullies develop in width and height with further annealing (Figure 1B,C). Some island structures resulted from decaying of continuous hills become rounder and rounder due to surface tension (Figure 1D,E). Finally, some droplets with bigger diameter can be obtained (Figure 1F). This scenario is in good agreement with dewetting pathway of SAN50 at 145 °C, which was called "fragment of bicontinuous structures". The only difference between them is that dewetting takes place faster at 155 °C due to the higher activity of polymer chains resulting from higher temperature.[19]

Figure 2 shows *in situ* AFM results of SAN70 at 155 °C. At the beginning, there are some holes (Figure 2A). These holes develop slowly in diameter and depth while some new holes with smaller diameter appear (Figure 2B,C). As a result, the number of holes per unit area increases and merger of these holes is unavoidable (Figure 2D,E). This kind of merger of several neighboring holes in certain direction isolates the film surrounded by them and produces some islands (shown as ellipse in Figure 2F). Finally, these islands become rounder and rounder, leading to the occurrence of droplets. This process is so similar to the transitional dewetting pathway in our previous work.[19] In the conclusion of that work, it is magnitude of U_{q0}/E that determines dewetting pathway. For film with higher U_{q0}/E (e.g., SAN50 at 145 °C), it dewets by means of "fragment of bicontinuous structures", while it undergoes "expansion of holes" for film with lower U_{q0}/E (e.g., SAN90 145 °C). Of course, SAN70 dewets in

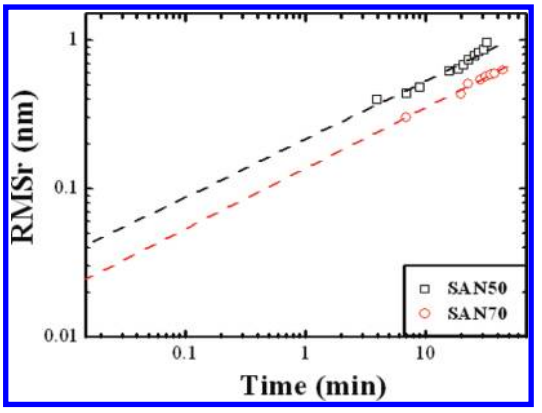

Figure 3. Annealing time dependence of *RMSr* (root-mean-square roughness) and its extrapolation for SAN50 and SAN70 at 155 °C.

the transitional pathway. In this work, $U_{q0,SAN50}$ is higher than $U_{q0,SAN70}$, which is obtained by fitting and extrapolating root-mean-square roughness (*RMSr*) as a function of annealing time in logarithmic scale (shown in Figure 3). This is the reason for different dewetting pathway in SAN50 and SAN70 since film thickness (E) of them is almost the same. In other words, dewetting pathways of SAN50 and SAN70 at 155 °C are still under the control of U_{q0}/E.

To investigate dewetting kinetics which follows the power law of $q^* \propto t^{-n}$ where q^* and t denote characteristic wavenumber of the topography images and annealing time, respectively, annealing time dependence of q^* is shown in Figure 4. One point to be noted is that result of SAN50 has been published.[18] On the basis of the dependence of the exponent n on the annealing time, three regimes in the development of characteristic wave vector were obtained in our results. Initially, n is almost independent of annealing time ($n \approx 0$). After that, n becomes 0.18 (in SAN50)

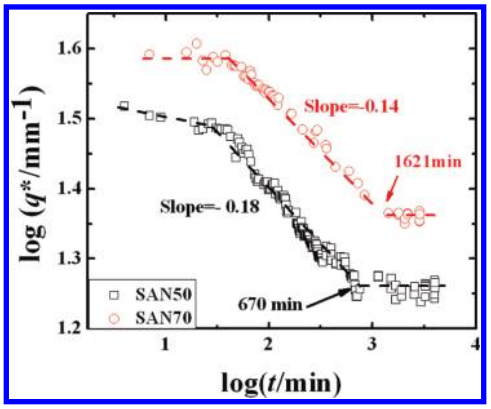

Figure 4. Characteristic wavenumber (q^*) computed from the topography images of a 2 × 2 μm^2 area for film (SAN50 and SAN70) annealed at 155 °C VS. annealing time on a logarithmic−logarithmic scale.

and 0.14 (in SAN70). They are in good agreement with the exponent of *RMSr* in dewetting of SAN50 (n = 0.17) and SAN70 (n = 0.15) at 145 °C[19,22] and different from 1/3 controlled by diffusion and 0.43 for polystyrene (PS) on a silicon substrate.[28−30] Finally, the exponent is independent of annealing time again, which indicates that dewetting is finished. The crossovers of three regimes in SAN50 and SAN70 are at $q^* = 30.55\ \mu m^{-1}$ (t = 34 min), $q^* = 18.20\ \mu m^{-1}$ (t = 670 min) and $q^* = 39.81\ \mu m^{-1}$ (t = 38 min), $q^* = 23.17\ \mu m^{-1}$ (t = 1621 min), respectively, indicating that dewetting structures develop slowly and it takes longer time to reach stable dewetted structures in SAN70 (1621 min) than SAN50 (670 min).

GIUSAX experiments were performed to detect phase-separated structures in our samples.[31,32] In Figure 5, lines are results of GIUSAX while black square curve is obtained from fast Fourier transition (FFT) from AFM images (Figures 1F and 2F). For the reason for comparison, they are shifted in the direction of intensity proportionally. In Figure 5A, there is only one peak at $q = 0.026\ nm^{-1}$ (red line, annealing for 1 h), which moves to the direction of lower q with further annealing (green line, annealing for 10 h). The second peak at $q = 0.061\ nm^{-1}$ comes into being at 24 h (dark blue line). Along with movements to the direction of lower q, intensity of this peak increases when our sample is annealed for 48 h (light blue line). On the other hand, FFT curve shows the correlation of droplets resulted from dewetting. From comparison of light blue line and square curve in Figure 5A, it is clear that there is only one peak in FFT curve at $q = 0.016\ nm^{-1}$, which is a representation of correlation among droplets in AFM image of Figure 1F. This peak is in good agreement with the peak at $q = 0.015\ nm^{-1}$ in the GIUSAX result (light blue line). However, there is the second peak at $q = 0.051\ nm^{-1}$ in the GIUSAX result at 48 h, which does not exist in the FFT curve. As shown in many reports,[19,33] this peak was caused by phase-separated structure (PMMA-rich and SAN-rich phases here) in the droplets. This result indicates that there is no phase-separated structure until our sample is annealed for 24 h. Phase-separated structures develop, leading to the increase of scattering intensity and movements of the GIUSAX peak to lower q direction at 48 h (light blue line in Figure 5A). In the GIUSAX result of SAN70 (Figure 5B), the intensity of peak is so low that it is hard to find it at 1 h (red line in Figure 5B). It ($q = 0.022\ nm^{-1}$) is strengthened when our sample is annealed for 10 h (green line). This peak moves to lower q direction with further annealing (dark blue

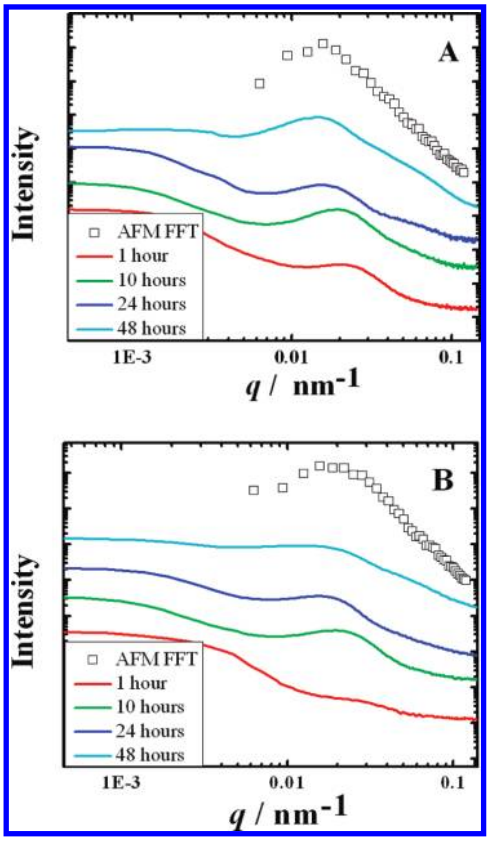

Figure 5. Common double-logarithmic presentations in reciprocal space of GIUSAX of samples SAN50 (A) and SAN70 (B) annealed at 155 °C for different time. Lines are results of GIUSAX, and black square curves are the fast Fourier transition (FFT) from AFM images of Figures 1F and 2F.

line). Furthermore, the second peak at $q = 0.049\ nm^{-1}$, which is caused by phase separation in droplets, comes into being at 48 h (light blue line). These results show that phase-separated structures of PMMA-rich and SAN-rich phases are detected when our sample is annealed for 48 h. From discussion above, phase separation of PMMA and SAN takes place both in SAN50 and SAN70. Furthermore, it occurs earlier in SAN50 although the quench depth of them is similar (there is phase separation at 155 °C and no phase separation at 145 °C in SAN50 and SAN70). This result is in good agreement with results in films (>10R_g) and bulk, in which phase separation takes place and develops faster in the critical component.[34−37]

As a matter of fact, there must be the competition and influence of phase separation and dewetting in polymer blend ultrathin films since they take place in the same system.[24] From the discussion of dewetting kinetics (Figure 4), it is clear that after the first regime dewetting develops fast, leading to the rapid decrease of q^*. Then, characteristic wave vector remains stable. In other words, dewetted structures remain stable after 670 and 1621 min in SAN50 and SAN70, respectively. On the other hand, it is worth to notice that phase-separated structures cannot be detected by GIUSAX until our samples are annealed for 24 h (1440 min) and 48 h (2880 min) in SAN50 and SAN70, respectively (Figure 5A,B). According to the discussion above, we can describe the interplay between phase separation and dewetting in SAN50 and SAN70 as follows: when the spin-coated PMMA/SAN film is heated to above their glass transition

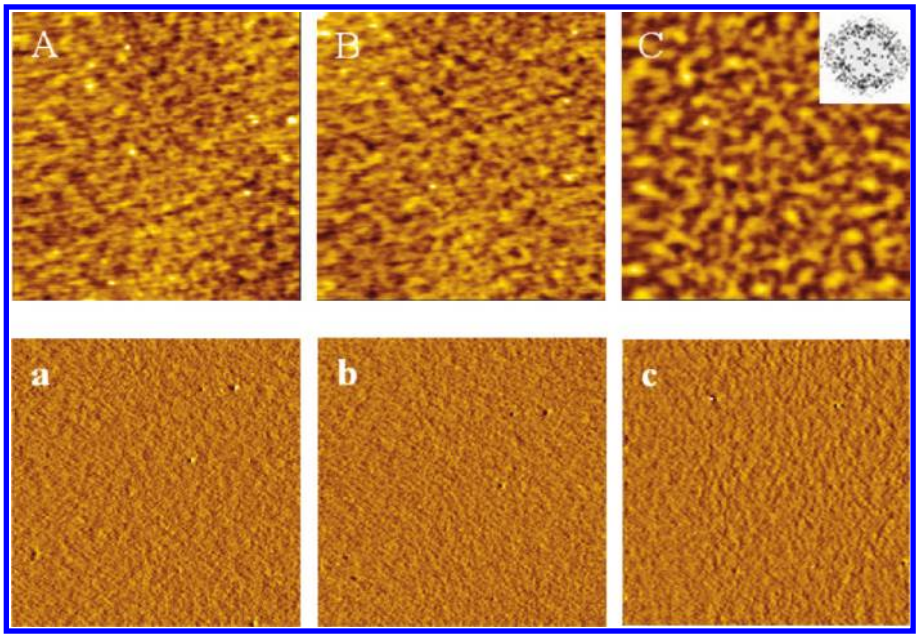

Figure 6. Snapshots of topography and phase images for sample SAN30 at 145 °C for 74 min (A and a), 161 min (B and b), and 2163 min (C and c). The *z*-axes for topography and phase images are 7.6 nm and 1.8°, respectively. Inset of image C is fast Fourier transform (FFT) from the corresponding image. The dimensions of all images are 2 × 2 μm^2.

temperature, PMMA diffuses to the substrate so as to create the composition gradient due to the favorable interaction with substrate.[38] Since this diffusion cannot take place precisely in the same way over the whole film, this is likely to create fluctuation of composition along the surface. When the amplitude of fluctuation is large enough, the free surface will be destabilized eventually.[17,19] This is so-called dewetting induced by composition fluctuation which has been predicted by theory and validated by experiment, respectively.[17−19] Upon heating to above critical temperature of our system, both dewetting and phase separation take place. However, the former occurs first due to the higher relative rate.[19,22] Some bicontinuous structures or holes (dependent on the magnitude of U_{q0}/E) develop with further annealing. As a result, some droplets are obtained. Finally, the correlation among these droplets remains stable, indicating that dewetting has been finished. After that, phase-separated structures are detected by GIUSAX at 24 h (in SAN50) and 48 h (in SAN70). In other words, phase-separated structures are detected in dewetted droplets after dewetting of the whole blend film is finished. During the above process, movement of PMMA chains to the substrate is unavoidable and acts as the foundation stone of composition fluctuation. This scenario is in good agreement with the mechanism of dewetting/wetting−phase separation which was discussed in the film thickness dependence of this interplay.[22]

Phase Behaviors in SAN30. Figure 6 shows the AFM snapshots of SAN30 annealed at 145 °C for different times. In topography images, there are some mimic-bicontinuous structures at 74 min (Figure 6A). They develop in width and height (Figure 6B) and decay into some island structures (Figure 6C). Inset is the fast Fourier transition (FFT) from the corresponding AFM image. During this process, *RMSrs* obtained by commercial software equipped on AFM are 0.41 nm (at 74 min), 0.48 nm (at 161 min), and 0.75 nm (at 2163 min). They are much lower than the result of SAN50 at 155 °C (5.36 nm) and 175 °C (7.42 nm) in our previous work,[18] in which the whole blend film of SAN50 dewetted and the substrate was exposed. On the other hand, phase images are homogeneous from first to last (Figure 6a−c), which is also different with the result of SAN50. Several points can be obtained from the evolution of phase images: first, phase separation does not take place due to the lower temperature; second, influence of height on phase images can be ignored since *RMSr* (<1 nm) is much lower compare to the radius of curvature of our tip (∼10 nm); last but not least, our substrate is still covered by polymer films.

Figure 7 shows the snapshots of topography and phase images of SAN30 after different annealing time at 155 °C. In topography images, we can find a similar but faster process compare to SAN30 at 145 °C. Several stages are included in the process: occurrence of (mimic-)bicontinuous structures, development of them, decaying into island, and formation of droplets. However, phase images evolve in a different way. The phase image is homogeneous when the film is annealed for 16 min. From then on, some darker domains occur and become more and more obvious. From the careful comparison between topography and phase images, it is clear that brighter droplets in topography images correspond to darker domains in phase images. The phase contrast between darker and brighter regions in phase images is ∼2.6°, which is in good agreement with the contrast between PMMA-rich and SAN-rich phase (∼2.5°) resulting from surface phase separation investigated by *in situ* AFM in the same condition[39] and much lower than that between polymer melt (PMMA/SAN) and substrate of silicon at 175 °C (∼110°).[18] Furthermore, the darker domain in phase images is PMMA-rich phase while continuous phase is SAN-rich phase according to the identification of domains at high temperature in vacuum.[39] By the commercial software equipped on AFM, it is very easy to calculate the volume of PMMA on the surface. In Figure 7F, mean height and diameter of droplets are 6.9 and 101.5 nm, respectively. Furthermore, there are 136 droplets in our image. Then, we can obtain the volume of these droplets (∼1.0 × 10^6 nm^3), which is 3.6% of the whole PMMA volume before annealing (∼2.7 × 10^7 nm^3). This discussion makes it clear that

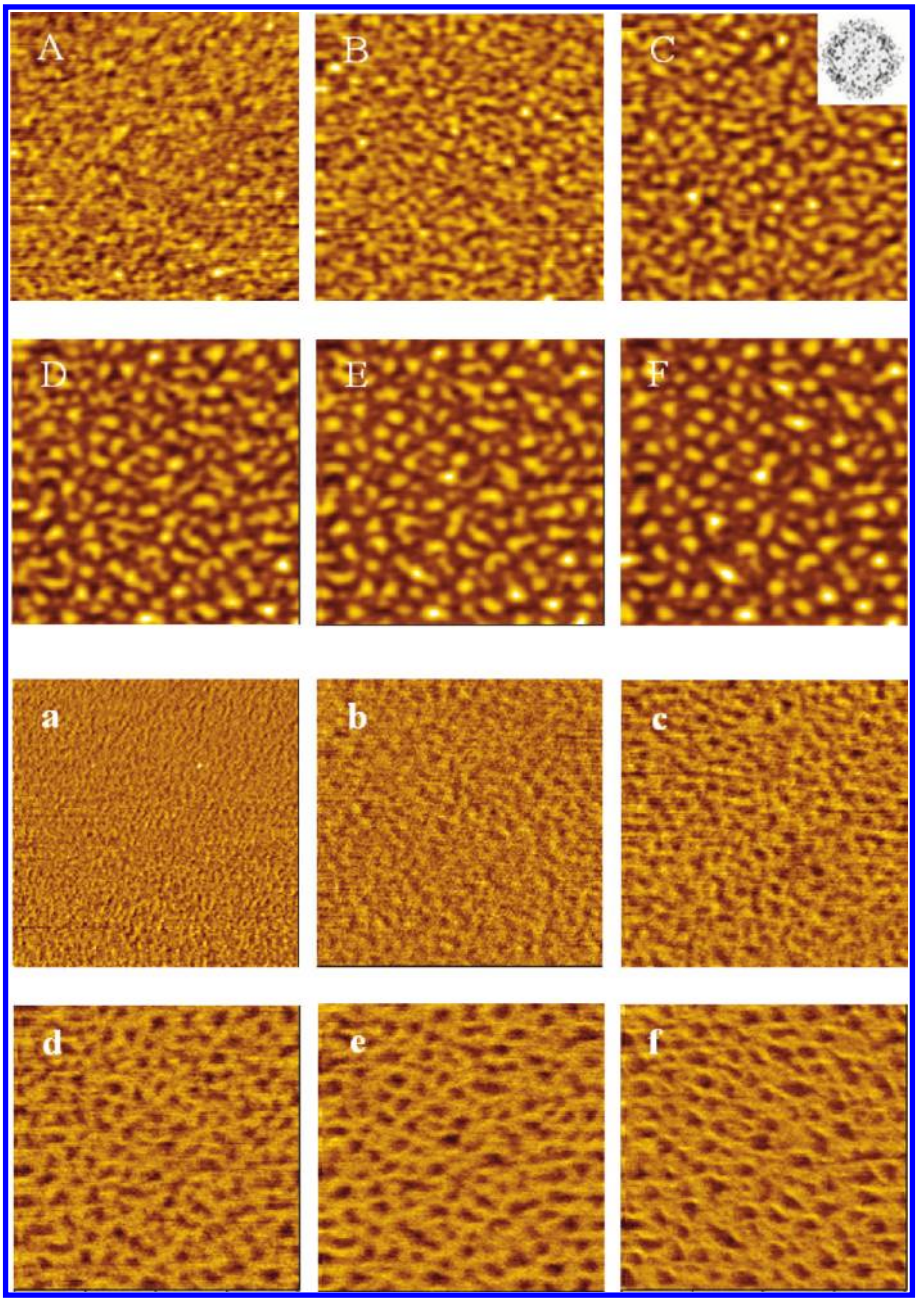

Figure 7. Snapshots of topography and phase images for sample SAN30 at 155 °C for 16 min (A and a), 68 min (B and b), 187 min (C and c), 630 min (D and d), 1296 min (E and e), and 4678 min (F and f). The *z*-axes for topography and phase images are 13.4 nm and 5.1°, respectively. Inset of image C is fast Fourier transform (FFT) from corresponding image. The dimensions of all images are 2 × 2 μm^2.

only a very small account of PMMA is on the surface. In this case, where is the rest of PMMA? It is worth to notice that interaction between PMMA and substrate is stronger than that of SAN, leading to the movement of PMMA to the substrate, which is the foundation stone of dewetting induced by composition fluctuation.[40] There must be some PMMA at the interface of substrate and polymer. In short, when spin-coated PMMA/SAN ultrathin films, with a surface excess of PMMA on the surface, is heated at 155 °C, PMMA diffuses to the substrate due to the favorable interaction between them. However, there is still some extra PMMA left on the surface due to two reasons: first, there is enough PMMA in SAN30 (means 70 wt % in this sample); second, surface tension of PMMA and SAN is nearly equal at this temperature, leading to the absence of both PMMA and SAN wetting layer.[41] Therefore, we can describe this interplay process as "wetting−dewetting/phase separation".

Composition Dependence of Phase Behaviors. To assess the stability of polymer films on the substrate, we can calculate the effective Hamaker constant (A_{eff}) by eq 1:

$$A_{eff} = (\sqrt{A_{substrate}} - \sqrt{A_{polymer}})(\sqrt{A_{air}} - \sqrt{A_{polymer}}) \quad (1)$$

where A is the Hamaker constant. According to the calculation of A_{eff}, it is clear that both PMMA and SAN films on the substrate are stable ($A_{PMMA} = 2 \times 10^{-20}$ J, $A_{SAN} = 0.8 \times 10^{-20}$ J, $A_{SiO} = 2.2 \times 10^{-20}$ J, and $A_{air} = 0$ J[42,43]). In the PMMA/SAN blend ultrathin film, however, it dewets the substrate by means

dx.doi.org/10.1021/ma200082m |*Macromolecules* 2011, 44, 5318–5325

of composition fluctuation. We can describe it as follows. For the PMMA/SAN blend film prepared by spin-coating, there is a surface excess of PMMA due to the higher solubility of PMMA in the solvent of 1,2-dichloroethane.[44] PMMA and SAN chains are frozen into a narrow zone before reaching a thermodynamically stable states since the solvent evaporates relatively fast during spin-coating.[41] When it is annealed at high temperature, there are several kinds of phase behavior including phase separation, wetting of PMMA on the substrate, dewetting of polymer film on substrate, and dewetting of one polymer on the other. Interplay among these behaviors is mainly controlled by relative rate of them.[22] Furthermore, many interplay mechanisms which look incongruous are the embodiment of it. They can coexist in one system and be changed from one to another by varying relative rate of them. In this work, phase-separated structures are detected after correlation among dewetted droplets remains stable in SAN50 and SAN70. In SAN30, however, dewetting of the whole film is suppressed.[45] Phase separation of the blend and dewetting of PMMA-rich phase on the polymer film accompany each other after the movement of PMMA to the substrate. It is quite clear that both phase separation and dewetting are affected by composition (SAN30 changed to SAN50 and SAN70) in the blend, resulting in the great difference of final structure, kinetics and interplay between them. Now, we try to clarify the composition dependence of them in two cases. For convenience, we label experiment temperature, glass transition temperature in ultrathin film, and critical phase separation temperature in ultrathin film as T, T_g, and T_c, respectively.

Case 1: $T_c > T > T_g$. When the sample is heated to above T_g but below T_c, polymer (e.g., PMMA) chains are active. There are two directions for PMMA: first, it will move to the surface to minimize free energy of the system if surface tension of it is much lower than that of SAN; second, it should move to the substrate if there is more favorable interaction with it than SAN. In the former case, dewetting of the whole film induced by composition fluctuation will not happen due to the absence of suitable composition gradient. In our system, surface tension of PMMA is nearly equal with that of SAN.[41] Furthermore, interaction between PMMA and substrate is stronger than that of SAN.[40] Therefore, PMMA prefers to move to the substrate, leading to composition gradient of it in the film thickness direction. In SAN50 and SAN70 at 145 °C, our system matches composition fluctuation theory very well. Therefore, U_{q0}/E was employed to distinguish different dewetting pathways.[22] Two kinds of dewetting pathway and transition between them obtained by varying component (SAN50, SAN90, and SAN70) have been reported.[19] In SAN30, however, there is enrichment of PMMA both on the surface and at the interface since PMMA is enough. As a result, some PMMA is left on the surface except the diffusion to substrate. This disturbs the gradient of it although it is only a very small account of PMMA (~3.6%). There is only fluctuation on the surface, not real dewetting. This is the reason for the very low magnitude of surface roughness (Figure 6C). In other words, dewetting of SAN30 film is suppressed due to the disturbed composition gradient at 145 °C.

Case 2: $T > T_c$. Because of the higher temperature above T_c, phase separation of the blend will take place and increase the activity of polymer chains, leading to more complicated interplay. When samples are heated, PMMA trends to diffuse to the substrate due to stronger interaction with silicon. As a result, the composition gradient of it will be obtained, which is followed by wetting layer of PMMA at the interface of substrate or dewetting of the whole films. Competition between them depends on the intensity of the gradient; that is, dewetting (wetting) will take place first if the intensity is very high (low). For instance, the whole film deweted the substrate and substrate was exposed due to the very high intensity in critical component (SAN50) at high temperature (175 °C),[18] followed by phase separation in droplets and formation of PMMA wetting layer on the substrate. In SAN50 and SAN70 at 155 °C, however, wetting layer of PMMA occurs accompanied by dewetting of film since gradient intensity is not very high due to low temperature. Subsequently, it is the problem of their interplay and competition with phase separation, which is controlled by relative rate of them.[22] From the comparison of kinetics of dewetting and GIUSAX result, it is clear that dewetting takes place before phase separation in SAN50 and SAN70 with this thickness (~$1R_g$). This is so-called dewetting/wetting−phase separation. In SAN30, these phase behaviors interplay in a different way. When it is annealed at 155 °C, partial PMMA diffuses to the substrate while some extra PMMA is left on the surface (Figure 7c−f). As discussed in case 1, this disturbs the composition gradient, namely, the foundation stone of dewetting induced by composition fluctuation. Therefore, dewetting of the whole film is suppressed. On the other hand, enrichment of PMMA on the surface leads to a further excess of it, resulting in the occurrence of phase separation since our sample is annealed above T_c. After that, phase-separated PMMA-rich phase dewets on the polymer film since A_{eff} of PMMA on SAN is positive according to eq 1. This is the reason why phase contrast in AFM phase images is similar to the contrast between PMMA and SAN. In this process, wetting of PMMA layer at the interface occurs first, which is followed by phase separation accompanied by dewetting of phase-separated PMMA-rich phase. This is the so-called "wetting−dewetting/phase separation".

CONCLUSION

In this work, the composition dependence of phase behaviors in PMMA/SAN blend ultrathin films with different components was investigated by *in situ* AFM and GIUSAX. It was found that dewetting pathways of SAN50 and SAN70 were still under the control of U_{q0}/E. Furthermore, phase-separated structures in dewetted droplets were detected by GIUSAX after the correlation among droplets remained stable. In SAN30, however, wetting of PMMA layer on the substrate occurred first, which was followed by phase separation and dewetting of the phase-separated PMMA-rich phase. In conclusion, phase behaviors including phase separation, dewetting, and interplay between them can be affected by varying component in the blend. Furthermore, this effect is carried out by means of influence on composition gradient. Our results are significant for controlling structures and properties in ultrathin polymer blend films.

AUTHOR INFORMATION

Corresponding Author

*E-mail tfshi@ciac.jl.cn, Tel +86-431-85262137, Fax +86-431-85262969 (T.S.); e-mail ljan@ciac.jl.cn, Tel +86-431-85262201, Fax +86-431-85685653 (L.A.).

ACKNOWLEDGMENT

This work is supported by the National Natural Science Foundation of China (50973110) Programs and the Fund for

Creative Research Groups (50921062) and subsidized by the Special Funds for National Basic Research Program of China (2010CB631100). T. F. Shi thanks Shanghai Synchrotron Radiation Facility project (10sr0169). We thank Dr. Zhiyong Jiang, Jianqi Zhang, Shanshan Hu, A. Timmann, and S. V. Roth for assistance in GIUSAX at HASYLAB.

REFERENCES

(1) Koh, K.; Sugiyama, S.; Morinaga, T.; Ohno, K.; Tsujii, Y.; Fukuda, T.; Yamahiro, M.; Iijima, T.; Oikawa, H.; Watanabe, K.; Miyashita, T. *Macromolecules* **2005**, *38*, 1264.
(2) Yeo, B. S.; Amstad, E.; Schmid, T.; Stadler, J.; Zenobi, R. *Small* **2009**, *5*, 952.
(3) Thickett, S. C.; Harris, A.; Neto, C. *Langmuir* **2010**, *26*, 15989.
(4) Jung, H. J.; Shin, Y. J.; Park, Y. J.; Yoon, S. C.; Choi, D. H.; Park, C. *Adv. Funct. Mater.* **2010**, *20*, 2903.
(5) Umeda, M.; Uchida, I. *Langmuir* **2006**, *22*, 4476.
(6) Newby, B. Z.; Wakabayashi, K.; Composto, R. J. *Polymer* **2001**, *42*, 9155.
(7) Colombani, J.; Bert, J. *Phys. Rev. E* **2004**, *69*, 011402.
(8) Puri, S.; Binder, K. *Phys. Rev. Lett.* **2001**, *86*, 1797.
(9) Heier, J.; Kramer, E. J.; Revesz, P.; Battistig, G.; Bates, F. S. *Macromolecules* **1999**, *32*, 3758.
(10) Affrossman, S.; Henn, G.; O'Neill, S. A.; Pethrich, R. A.; Stamm, M. *Macromolecules* **1996**, *29*, 5010.
(11) Yeung, C. *Phys. Rev. Lett.* **1988**, *61*, 1135.
(12) Wu, Y.; Alexander, F. J.; Lookman, T.; Chen, S. *Phys. Rev. Lett.* **1995**, *74*, 3852.
(13) Toxvaerd, S. *Phys. Rev. Lett.* **1999**, *83*, 5318.
(14) Huh, J.; Park, C.; Kwon, Y. K. *J. Chem. Phys.* **2010**, *133*, 114903.
(15) Asfaw, M.; Chen, H. Y. *Phys. Rev. E* **2009**, *79*, 041917.
(16) Levine, J. R.; Cohen, J. B.; Chung, Y. W.; Georgopoulos, P. *J. Appl. Crystallogr.* **1989**, *22*, 528.
(17) Wensink, K. D. F.; Jérôme, B. *Langmuir* **2002**, *18*, 413.
(18) Liao, Y.; Su, Z.; Sun, Z.; Shi, T.; An, L. *Macromol. Rapid Commun.* **2006**, *27*, 351.
(19) You, J.; Hu, S.; Liao, Y.; Song, K.; Men, Y.; Shi, T.; An, L. *Polymer* **2009**, *50*, 4745.
(20) Sharma, A.; Khanna, R. *Phys. Rev. Lett.* **1998**, *81*, 3463.
(21) Sharma, A.; Khanna, R. *J. Chem. Phys.* **1999**, *110*, 4929.
(22) You, J.; Liao, Y.; Men, Y.; Shi, T.; An, L. *Langmuir* **2010**, *26*, 14530.
(23) Tanaka, K.; Yoon, J. K.; Takahara, A.; Kajiyama, T. *Macromolecules* **1995**, *28*, 934.
(24) Ogawa, H.; Kanaya, T.; Nishida, K.; Matsuba, G. *Polymer* **2008**, *49*, 254.
(25) Hansen, J.; Reatto, L.; Tau, M.; Victor, J. *Mol. Phys.* **1985**, *56*, 385.
(26) Lietor-Santos, J.; Kim, C.; Lynch, M.; Fernandez-Nieves, A.; Weitz, D. *Langmuir* **2010**, *26*, 3174.
(27) Newby, B. Z.; Composto, R. J. *Macromolecules* **2000**, *33*, 3274.
(28) Xie, R.; Karim, A.; Douglas, J. F.; Han, C. C.; Weiss, R. A. *Phys. Rev. Lett.* **1998**, *81*, 1251.
(29) Gleiche, M.; Chi, L. F.; Fuchs, H. *Nature* **2000**, *403*, 173.
(30) Higgins, A. M.; Jones, R. A. L. *Nature* **2000**, *404*, 476.
(31) Müller-Buschbaum, P.; Cubitt, R.; Petry, W. *Langmuir* **2003**, *19*, 7778.
(32) Lee, B.; Yoon, J.; Oh, W.; Hwang, Y.; Heo, K.; Jin, K. S.; Kim, J.; Kim, K. W.; Ree, M. *Macromolecules* **2005**, *38*, 3395.
(33) Müller-Buschbaum, P.; Gutmann, J. S.; Stamm, M.; Cubitt, R.; Cunis, S.; Krosigk, G. v.; Gehrke, R.; Petry, W. *Physica B* **2000**, *283*, 53.
(34) Tanaka, H. *Phys. Rev. Lett.* **1994**, *72*, 3690.
(35) Tanaka, K.; Takahara, A.; Kajiyama, T. *Macromolecules* **1998**, *31*, 863.
(36) Colombani, D.; Chaumont, P. *Macromolecules* **1994**, *27*, 5972.
(37) Ermi, B. D.; Nisato, G.; Douglas, J. F.; Rogers, J. A.; Karim, A. *Phys. Rev. Lett.* **1998**, *81*, 3900.
(38) Liao, Y.; You, J.; Shi, T.; An, L.; Dutta, P. K. *Langmuir* **2007**, *23*, 11107.
(39) Liao, Y.; Su, Z.; Ye, X.; Li, Y.; You, J.; Shi, T.; An, L. *Macromolecules* **2005**, *38*, 211.
(40) Wang, H.; Composto, R. J. *Interface Sci.* **2003**, *11*, 237.
(41) You, J.; Shi, T.; Liao, Y.; Li, X.; Su, Z.; An, L. *Polymer* **2008**, *49*, 4456.
(42) Sferrazza, M.; Xiao, C.; Jones, R. A. L.; Bucknall, D. G.; Webster, J.; Penfold, J. *Phys. Rev. Lett.* **1997**, *78*, 3693.
(43) Ono, H.; Sato, F.; Jidai, E.; Sbibayama, K. *Colloid Polym. Sci.* **1975**, *253*, 538.
(44) Li, Y.; Yang, Y.; Yu, F.; Dong, L. *J. Polym. Sci., Part B: Polym. Phys.* **2006**, *44*, 9.
(45) Müller-Buschbaum, P.; Gutmann, J. S.; Stamm, M. *Macromolecules* **2000**, *33*, 4886.